Dissociative Energy Flow, Vibrational Energy Redistribution, and Conformeric Structural Dynamics in Bifunctional Amine Model Systems†

Joseph C. Bush, Michael P. Minitti, and Peter M. Weber*

Department of Chemistry, Brown University, Providence, Rhode Island 02912

Received: March 02, 2010; Revised Manuscript Received: May 20, 2010

Time-resolved multiphoton ionization mass spectrometry coupled with Rydberg Fingerprint Spectroscopy (RFS) has been used to analyze the structural and electronic dynamics of *N*,*N*-dimethylphenethylamine (PENNA) and *N*,*N*-dimethylcyclohexethylamine (CENNA). In PENNA, the molecule converts from 3p to 3s on a time scale of 149 fs, a process that is reflected in the mass spectrum as the onset of fragmentation. Once in 3s, the overall signal intensity of the PENNA 3s signal shows biexponential decay kinetics, which is attributed to the electronic curve crossing from the Rydberg state to a dissociative antibonding orbital of the ethylenic bridge. This curve crossing exemplifies a possible fragmentation pathway observed in electron capture dissociation of proteins. The initially fast reaction (1.3 ps) is greatly slowed down as a result of an apparent relaxation process with a 5.6 ps time constant. The electron binding energy of the 3s Rydberg state of PENNA is observed to shift with a time constant of 4.8 ps, which is correlated to a cation$-\pi$ interaction driven conformeric rearrangement.

Introduction

The interplay of vibrational energy flow, conformeric motions across complex potential energy landscapes, and highly excited (possibly crossing) electronic states determines the nonstatistical outcome of electron capture dissociation (ECD) processes[1] that are widely observed in mass spectrometry of proteomic systems. Alternative techniques, such as collision induced dissociation (CID)[2] and infrared multiphoton dissociation (IRMPD),[3] deposit energy in the molecule in a thermal distribution, spreading energy statistically over the many modes of the system. This leads to predictable fragmentation patterns where the most labile bonds are preferentially broken, typically producing *b*, *y* fragments.[4,5] Under the conditions of ECD, however, where low kinetic energy electrons are attached to polycationic molecules, different fragmentation pathways are observed. The dominant fragmentation products result from cleavage of disulfide and N−C bonds, to give *c* and *z* fragments, where generation of both of these fragments has been shown to be independent of temperature.[1] This apparent break from ergodic energy distribution[1] represents a distinctly different pathway for energy transfer than conventional thermal modes. The mechanism for the formation of dissociation products from ECD has been the subject of much debate, and even whether it represents nonstatistical behavior has been debated.[6] The positive charge centers of ECD analytes are typically protonated amines generated during the electrospray process. The postulated mechanisms can be summarized in two different ways: (1) electron capture to an electrophilic site followed by a reaction cascade mechanism[7] and (2) electron capture to a Rydberg state followed by energetic condensation through a conical intersection or electronic curve crossing.[8−11] The validity of the proposed mechanisms is largely dependent on the coupling strength between Rydberg states and antibonding orbitals of specific bonds of the molecular skeleton. Other factors that play significant roles are the redistribution of vibrational energy, excited state lifetimes, as well as conformeric motions of the molecular systems.

In the present work, we explore model systems of minimally necessary complexity. The localized and highly selective nature of ECD suggests that even comparatively small molecular models may enable us to capture the essential processes at work. Proteins and peptides are composed of amino acids, each with their characteristic side chains, connected to an amide backbone. These functional groups have distinct physical properties such as basicity and UV-absorption, while being physically tethered in close proximity. The electron density of the nitrogen and acyl oxygen in the amide bond is delocalized[12] and forms a near degeneracy between the n_O and π_2 orbitals.[13]

To test the validity of the proposed ECD mechanisms, we have chosen a model system with two functional groups, similar to amino acid side chains, yet without the amide backbone, thus avoiding complications from overlapping electronic manifolds. *N*,*N*-Dimethylphenethylamine (PENNA) and its hydrogenated counterpart *N*,*N*-dimethylcyclohexethylamine (CENNA) support positive charges at the amine moiety and feature an α C−C bond that easily fragments, similar to the fragmentation observed in peptides. PENNA consists of two photophysically distinct chromophores separated by an ethyl spacer, which allows for site-selective photoexcitation.[14] PENNA has been used as a model for small peptides previously.[15,16] Weinkauf has calculated the equilibrium structures of the neutral and cation as well as the extent of charge delocalization of a positive charge between the amine and the aromatic ring.[17] PENNA has been shown to exhibit charge transfer from the benzene ring to the amine after selective ionization[17] according to a donor−bridge−acceptor model.[18] This process has been shown to flow spontaneously and on very short time scales.[19] The existence of an electronic state in close proximity energetically and within the nuclear coordinate phase space to the initially populated state allows for the rapid interconversion between the states and charge transfer from the phenyl to the amine. Similar donor−bridge−acceptor-type transfers have been observed in other systems over larger distances.[20] CENNA, having the same photoactive amine

† Part of the "Klaus Müller-Dethlefs Festschrift".

* Corresponding author. E-mail: peter_weber@brown.edu.

10.1021/jp101881x
Published on Web 07/01/2010

chromophore but lacking the aromatic ring functional group, is used as a reference case. It is particularly useful for a comparative evaluation of the conformational dynamics.

Experiments with time resolution in the subpicosecond regime typically require a well-defined event that induces a reaction and an investigative event that probes the progress of the reaction after a certain elapsed time. Electron capture by a free ion does not easily lend itself to such a pump−probe sequence. To make highly time-resolved experiments possible, we start with the neutral molecule instead of a positive ion, excite optically to a low-lying Rydberg state, and observe the ensuing dynamics using time-resolved photoelectron and mass spectroscopy. While this approach enables us to follow the energy flow in real time, we note that the amine ion core is a tertiary amine with an unpaired electron, which differs from the quarternary amine ions to which an electron is attached in ECD. Nevertheless, the insights gained from our study, especially as it pertains to the vibrational energy flow and conformeric reactions, can teach us about the processes in positively charged peptide chains.

Photoelectron spectroscopy has two important advantages for the observation of molecular dynamics. First, by measuring the binding energy of the molecule with an ultrashort ionization laser pulse, it provides an instantaneous snapshot of the molecular identity. Second, the analysis of the electron binding energy yields a unique fingerprint in which the molecular structure is encoded in the Rydberg electron binding energy.[21−23] Even in polyatomic systems, the so-called Rydberg Fingerprint Spectra (RFS) are remarkably sensitive to subtle changes in molecular structure, including conformation.[24,25] As the ionization transition from a Rydberg state to an ion state involves almost identical potential energy surfaces, the transitions are not broadened by vibrational structure, so that large amounts of internal energy do not affect the binding energy spectra.[26] The combination of high molecular shape sensitivity along with the high time resolution of the employed pump−probe methodology makes RFS an ideal probe of the structural part of the dynamics in PENNA and CENNA.

Mass spectrometry (MS) provides a further complementary view of the molecular dynamics. While it is tempting to identify the molecular species involved in the dynamics through their masses, it is important to realize that mass spectrometry measures the final outcome of a reaction sequence.[27] When the mass spectrometer detector is situated far from the ionization center, the ions can fragment on their way to the detector provided they have sufficient energy to do so. For well-identified molecular systems, mass spectrometry is therefore primarily a tool to determine how much energy the ionization process deposits into vibrational or electronic degrees of freedom.

Due to their complementary information content, we apply both RFS and MS to study the energy flow in our model systems. A photon with about 6 eV of energy lifts the molecule to the low-lying, $n = 3$, Rydberg states (Figure 1). Because this excitation is associated with the planarization of the tertiary amine group, the excitation step leads to the side of the well of the amine umbrella motion, depositing 0.86 eV of energy into the molecule when excited to 3p.[24] Either direct excitation or rapid electronic relaxation (τ_1 decay) from 3p to 3s can deposit an additional 1.52 eV of energy into vibrations. The highly energized molecules can now distribute their energy across all vibrational modes via intramolecular vibrational relaxation (IVR, decay time t_2), engage in structural rearrangements that lead to a cation−π bonded structure that eventually relaxes back to the ground state (A), or find the repulsive surface that splits the

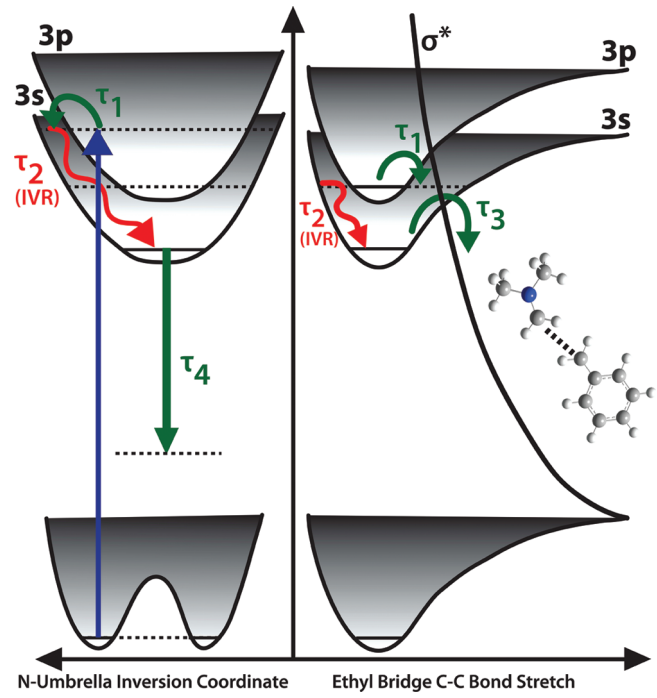

Figure 1. Energy diagram for RFS of PENNA. Photoexcitation at 208 nm (~6 eV) promotes an electron to either 3p or 3s and initially deposits vibrational energy locally at the amine site. The 3p state rapidly interconverts to 3s with a rate τ_1 and can then either cross the barrier to the σ^* state (τ_3) to produce neutral fragments, redistribute its vibrational energy over the entire molecule at a rate τ_2, or convert back down to the ground state, possibly by fluorescence (τ_4).

carbon−carbon bond in α position to the amine group (decay time t_3) leading to the formation of neutral fragments (F). The time-delayed photoionization spectrum, coupled with the mass spectrum, reveals the different aspects of those competing processes.

Experimental Considerations

The experimental setup has been described in detail previously and will only be described briefly.[28,29] Sample molecules were seeded in a helium carrier gas (1.2 bar), which undergoes adiabatic expansion into the high vacuum region of the spectrometer. The molecular beam crosses the laser interaction region perpendicular to the laser beams and to the time-of-flight corridor. Ions and electrons are detected by microchannel plates in a chevron configuration, which are connected to ultrafast timing electronics.

Femtosecond laser pulses are produced with a commercial Titanium-Sapphire laser (Spectra-Physics, Tsunami) and are amplified in a 5 kHz regenerative amplifier (Positive Light, Spitfire). The output of the amplifier can be tuned over a range of 800 ± 50 nm and has typical pulse durations of 150 fs and pulse energies of 200 μJ. The amplified near-IR output pulses are upconverted by sequential BBO crystals, providing the second harmonic (2ω, 414−418 nm) and fourth harmonic (4ω, 207−209 nm) that are used as the probe and the pump pulses, respectively.

PENNA was purchased from Sigma-Aldrich and used without further purification. CENNA was synthesized according to an adapted method of catalytic hydrogenation.[30] PENNA (7 g, 47 mmol, Sigma-Aldrich) was added to glacial acetic acid (100 mL) with Adam's catalyst (PtO_2, 1 g, 4.4 mmol). The solution was shaken under H_2 (50 psi, 14 h), filtered, and condensed.

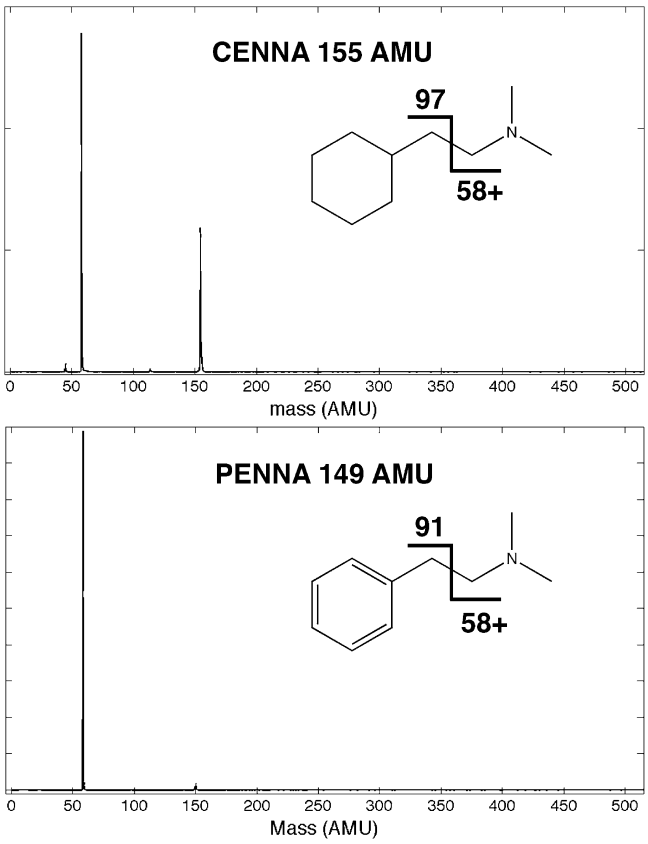

Figure 2. Mass spectra of CENNA, top, and PENNA, bottom, taken by two-color ionization with pulses at 208 and 416 nm, respectively. The spectra represent the averages over all time delays between the pump and probe pulses. The molecular structure indicates the dissociation of the α bond, which gives rise to the fragment ion at mass 58.

The residual was dried in ether over KOH and condensed to give the pure product as confirmed by ^{1}H NMR and MS.

Results and Discussion

The two-color photoionization mass spectra of PENNA and CENNA, time-averaged over all time delays, are shown in Figure 2. Both spectra show prominently the $N(CH_3)_2CH_2$ radical at mass 58, which arises from the fission of the carbon−carbon bond in the α position to the amine group. The mass spectra are free of any other fragment, reinforcing the well-known preponderance of this particular bond fracture in ionization spectra of tertiary amines. At the expansion conditions of this experiment, no van der Waals clusters are observed.

Figure 3 shows the time-resolved RFS spectra of both PENNA and CENNA. The binding energy is plotted in the range of 2−3 eV and the delay time up to 9 ps, representing the regime where the PENNA spectrum shows fascinating dynamics. By analogy with spectra of other tertiary amines,[31] we assign the short-lived features near 2.2 eV to the 3p states, while the longer-lived peaks near 2.8 and 2.9 eV are ascribed to the 3s states. A visual inspection of those spectra suggests that the 3p levels are initially excited by the laser pulse, but they decay into the 3s level on a subpicosecond time scale. However, a kinetic fit of the RFS features shows that the PENNA population is preferentially excited directly to the 3p with concurrent excitation to 3s at a ratio of 1.6:1. Importantly, the 3s feature of PENNA shows a unique time-dependent shape, which we investigate further below. In contrast, the 3s peak of CENNA remains steady, much as we have observed in other amines that lack further dynamics in 3s (e.g., trimethyl amine,[31] 1,4-dimethylpiperazine).

Analysis of Signal Intensities. A superposition of the time-dependent intensities of the 3p and 3s Rydberg levels of PENNA along with the detected mass spectral peaks, Figure 4, reveals that the time dependence of the parent peak at mass 149 is identical to that of the 3p electronic state. The molecule is excited to the 3p level from where subsequent ionization gives rise to ions that do not fragment on their path to the mass spectrometer detector. The 3p level quickly decays into 3s, with a time scale of 149 fs. The time dependence of 3s, in turn, mirrors the lifetime of the fragment peak of the mass spectrum. Apparently, the electronic transition from 3p to 3s converts enough energy into vibrational energy that once ionized the molecule can fragment on the way to the mass spectrometer detector. While the time-dependent mass spectrum of PENNA therefore reflects the transition from 3p to 3s, we note that in CENNA there is already enough energy when excited to 3p for fragmentation to occur: we only observe a rapid rise of the fragment signal, followed by a plateau that is insensitive to the decay from 3p to 3s that is evident in the photoelectron spectrum (Figure 3).

To understand the energy flow in PENNA upon generation in its Rydberg state, we note that the initial optical transition deposits 0.86 eV of energy into vibrational coordinates. Such a large deposition of vibrational energy within the optical excitation is possible because the amine group changes from a pyramidal to a planar shape, and the Franck−Condon factors for the excitation are largest for transitions with large vibrational amplitude. An additional 0.66 eV is deposited into vibrational energy as the molecule transitions from 3p to 3s. We conclude that the appearance energy for ion fragments must be between 0.86 and 1.52 eV, explaining the close correlation of the fragments with the electronic states.

Once populated on a subpicosecond time scale, the 3s level and the fragment ion signal of PENNA decay quite rapidly with a nonexponential form. This behavior is quite unique among the many tertiary amines that we have studied to date. Figure 5 displays the time-dependent photoelectron signal over a larger time interval. To fit the data, we use the kinetic model shown in the inset of Figure 5. The model posits that there are two pathways out of 3s, which decay using two distinct time scales: one decays on a fast time scale (k_3) that persists for only a few picoseconds, and another follows a slower time scale (k_4) that takes tens of picoseconds. The fit parameters are listed in Table 1.

To rationalize the model, we note that the entire 0.86 eV of vibrational energy that the molecule receives during optical excitation is initially inserted into the umbrella motion of the amine group. Because it is the amine group that carries the positive charge of the ion core, one can surmise that the additional vibrational energy resulting from the electronic curve jump would be localized there as well. We propose that just after the molecule is generated in 3s through the decay from 3p it has not had sufficient time to distribute the internal energy, or change its conformeric structure, so that the vibrational energy is localized at the amine ($3S_{loc}$). With a large amount of vibrational energy right near the dissociative potential energy surface of the α C−C bond, the molecule can, according to the hypothesis, effectively access this dissociative channel. This crossing to a dissociative channel must compete, however, with a rapid IVR or structural relaxation process that tends to delocalize the vibrational energy among all modes of the molecule, including the ring vibrations ($3S_{deloc}$). With the energy

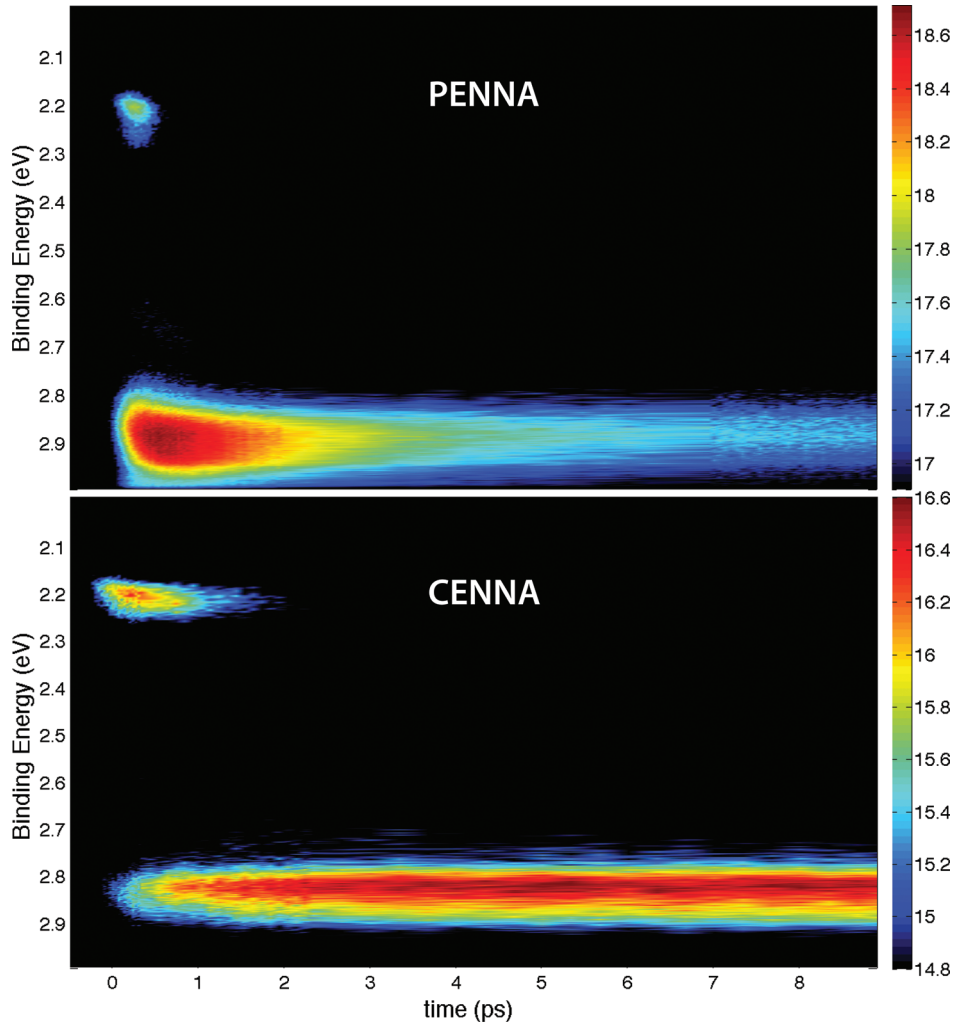

Figure 3. Time-resolved Rydberg Fingerprint Spectra, showing the time-dependent binding energy of the Rydberg electrons in PENNA (top) and CENNA (bottom). The logarithm of the intensity of the signal is decoded in the false color plots as indicated in the color bar on the right. Ionization was with pump pulses at 208 nm and probe pulses at 416 nm.

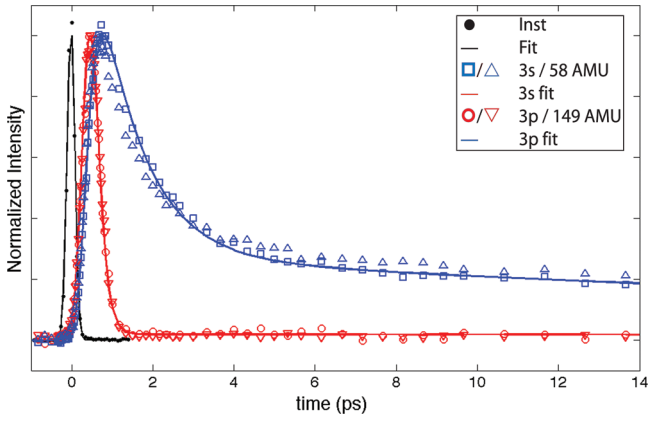

Figure 4. Time-dependent intensities of the RFS spectral features (solid lines) and the MS signals at 149 amu (parent) and at 58 amu (fragment) of PENNA. Due to the low cation dissociation energy, the 3p-to-3s decay directly reflects the cation dissociation, leading to an excellent agreement between the RFS and MS decay signals.

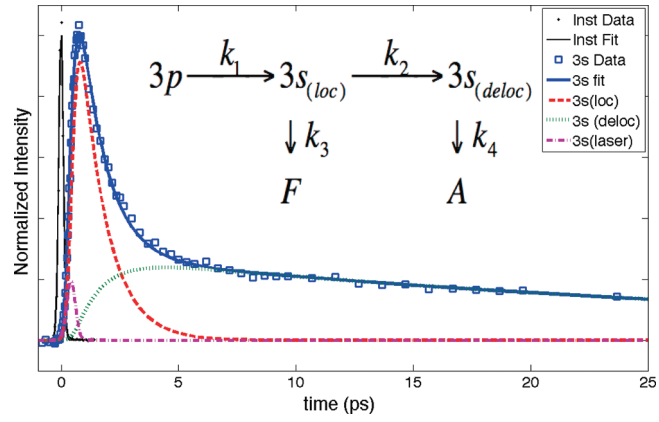

Figure 5. Fit of the PENNA 3s signal using the kinetics scheme shown in the inset. The observed 3s signal is taken to equal the sum of the 3s(localized) and 3s(delocalized) signals. The instrument function, arising from the cross correlation of the pump and the probe pulses, is at very early times ("Inst Data" and "Inst Fit").

delocalized over all of the molecule's vibrational degrees of freedom, or the structure of the molecule altered, access to the dissociative channel may be much less likely, giving rise to a decay with a slower time constant. We cannot distinguish a slow crossing to the dissociative state from a possible fluorescence decay or internal conversion process to a lower surface, so that the slow decay time (34 ps) encompasses them all. Of course, the pathways of energy relaxation could be more complicated than captured by the simple model. For example, the rate of the curve crossing reaction could change as energy drains out

TABLE 1: Fit Parameters of the Decay of the PENNA 3p and 3s Signals Using the Kinetics Scheme Shown in the Inset of Figure 5,a

	$1/k_1$	$1/k_2$	$1/k_3$	$1/k_4$
PENNA	149 fs	5.6 ps	1.3 ps	34 ps
CENNA	913 fs	-	-	-

[a] There is only one time constant for CENNA, k_1, which reflects the decay of 3p and simultaneous rise of 3s.

of the amine group. The excellent fit of the model to the experimental data does not warrant the inclusion of such complexity.

From the deconvoluted fits of the intensities of the RFS spectra, according to this model, we determine the rate of the curve crossing from S_{loc} to A to be 1.3 ps and the rate of energy distribution to be 5.6 ps. The integrated intensities of the long and slow fit components of the 3s signal show that under our experimental conditions 13% of the molecules do the curve crossing while 87% undergo vibrational energy redistribution. The signal intensities cannot distinguish between vibrational energy relaxation and structural transformations, but we will return to that point later.

The dissociation along the repulsive surface leads to ground state neutral molecules that could be ionized by the probe laser photons. It is plausible, but not necessary, that the curve crossing that depletes the 3s Rydberg state produces the mass 58 fragment that is observed in the mass spectrum. To search for other possible reaction products, we have performed RFS-MS experiments using significantly higher intensities of the ionizing laser pulse. We would expect to observe any newly generated fragment to be ionized by one-color multiphoton ionization using this probe pulse alone. However, we observed no new fragments in this experiment, leading us to conclude that it is, in fact, the α bond that dissociates through this curve crossing.

To further explore the nature of the curve crossing, we have investigated the effect of bond extensions on the amine moiety using NBO calculations with a 6-31G++(d) DFT basis set within the Gaussian 03 calculation package.[32] Structures used in the calculations were the minimum energy conformers found in structure optimizations for the neutral PENNA and CENNA. The initial neutral PENNA structure was the one found by Weinkauf.[17] Calculations were also performed using the local minimum structure of the cation with the planar amine group in anti position with respect to the phenyl ring. While calculations at such high electronic energies need to be interpreted with caution, they show that the σ^* orbital of the C−C bond in the ethyl bridge between the amine and phenyl becomes degenerate with the Rydberg 3p and 3s orbitals upon a bond extension of 2.16 and 2.3 Å, respectively, when the amine is planar. Since such bond extensions may be reachable when in excess of 0.86 eV (3p) and 1.52 eV (3s) of energy is concentrated in the amine moiety, it appears likely that indeed we observe the nonstatistical access of the repulsive bond as a transient phenomenon. Calculations on CENNA showed the σ^* states to be higher in energy than the corresponding states in PENNA by several hundred millielectronvolt, apparently leaving the curve crossing inaccessible to the CENNA Rydberg electron. One reason why in PENNA the σ^* state is lower than in CENNA may be that the phenyl radical can better accommodate the radical.

Analysis of the Electron Binding Energies. Separate from the signal intensities, RFS encodes the time-dependent molecular structure in the time-varying electron binding energy. A visual inspection of Figure 3 already shows that, at least for PENNA, the 3p signals are slanted and the 3s signal shifts with time. To

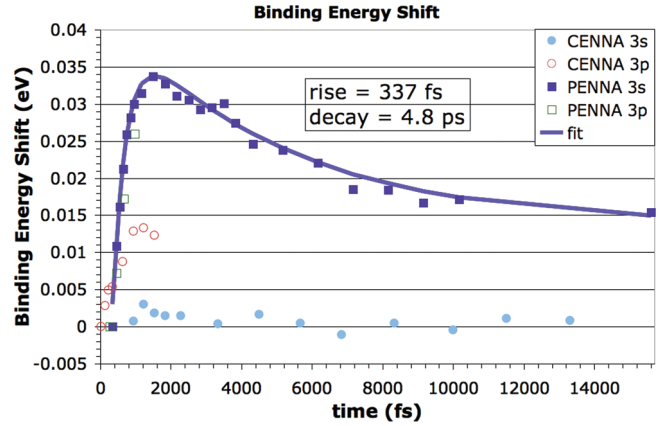

Figure 6. Time-dependent electron binding energies of the 3p and 3s Rydberg states of PENNA and CENNA upon excitation to the respective 3p states with 208 nm pulses.

quantify these shifts, we fitted the spectra in time slices to Gaussian line shapes and plotted the center positions as a function of pump−probe delay time (Figure 6). In PENNA, the 3p signal is measurable only over its short lifetime, during which it shifts by 28 meV toward higher binding energy. The 3s binding energy shifts upward by 30 meV in the first 1.25 ps with an approximate time constant of 337 fs but then turns around and decreases in an approximately exponential way with a time constant of 4.8 ps. On a similar time scale as the decay in binding energy, the PENNA 3s signal narrows in width by approximately 36%. In CENNA, whose 3p state has a longer lifetime (913 fs), the 3p center undergoes a shift of 13 meV to higher binding energies before internal conversion to 3s depletes the level. Once the electron is in 3s, CENNA shows no further variations in the electron binding energy, indicating that by that time all structural dynamics has completed and the molecules have reached their equilibrium distributions.

To interpret the RFS spectra, we recall that they encode the molecular structure in the binding energy and that vibrational motions do not broaden the spectral lines.[24] The origin of broadened lines lies in distributions of molecular structures about their equilibrium positions. This happens in molecules where rotations about single bonds give rise to multiple conformeric structures. In the systems discussed here, conformeric forms may arise from the rotation of the ethylenic single bonds, which rotate the amine group with respect to the rings. The methyl groups may also rotate about their C−N bonds, but previous studies have shown that the effect of these motions on the line widths is unobservably small.[24]

In PENNA and CENNA, we observe two separate structural dynamics time scales. The first is the rise in binding energy within the first picosecond, which is seen in both the 3p and 3s levels of PENNA and in the 3p state of CENNA. Similar rapid increases have been observed in other tertiary amines investigated in our laboratory, notably trimethylamine,[31] tripropylamine, triethylamine,[33] and dimethylpropylamine. Because all these systems have in common the time scales of the initial rise and the tertiary amine groups, we ascribe this initial shift toward higher binding energies to the planarization of the amine group upon excitation to the Rydberg manifold. This structural change may also be the source of difference between the observed 3p lifetimes of PENNA and CENNA. DFT calculations using a 6-311G++(d) B3LYP level of theory show the HOMO, which is localized on the amine, to penetrate into the phenyl ring upon planarization. This coupling could result in the faster internal conversion rate.

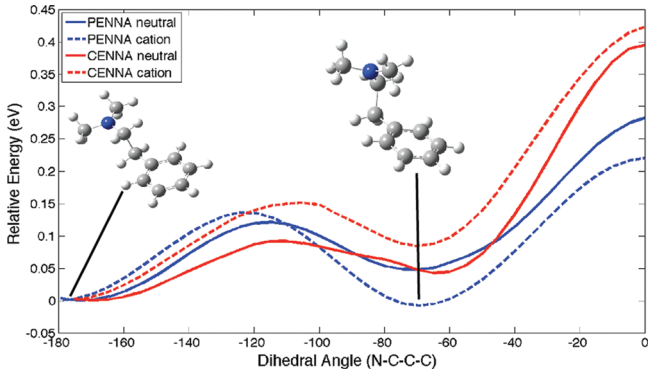

Figure 7. Potential energies of cationic PENNA and CENNA as a function of the dihedral angle corresponding to the rotation of the amine group toward the ring moiety using DFT B3LYP 6-31G+(d) theory. The molecular images shown are the structures of PENNA at the respective minima. In PENNA, the cation−π interaction leads to the formation of a deep well that is not present in the ground state neutral molecule, while in CENNA there is no corresponding stabilizing interaction.

The magnitudes of the 3p shifts are quite different for the two molecules: 25 and 13 meV for PENNA and CENNA, respectively. At present, we use the electron binding energies as relative indicators of the structural dynamics, so that we cannot yet interpret the absolute values of the shifts. There is no reason to suggest that the magnitudes of the shifts should be similar in the two systems. However, when the 3p and PENNA 3s shifts are normalized with respect to their overall magnitude, they show identical rise times (337 fs).

The second temporal evolution in the binding energy regime is seen only in the 3s level of PENNA, where the binding energy decreases by about 20 meV with an exponential decay constant of 4.8 ps. We ascribe this shift to the changing conformer distribution due to the creation of a new lowest-energy structure after excitation to the ion-like potential energy surface of the Rydberg manifold. In the molecular ground state, the initial distribution favors an extended structure with the amine group in anti position with respect to the phenyl ring.[17] Upon excitation to the Rydberg surface, a gauche structure, where the ethylene group rotates such that the amine group approaches the aromatic ring, is stabilized by an interaction between the positive charge center on the amine group and the delocalized π electron cloud of the ring (Figure 7). According to Weinkauf,[17] the neutral molecule has five minimum energy structures, whereas in the ion state only two minimum energy structures are found. Upon excitation to the Rydberg manifold, this structural distribution initially is projected onto the excited state surface, giving rise to the broad spectral features. Because the potential energy landscape, and the internal energy, on the ion-like Rydberg surface is dramatically different than in the ground state, the molecule readjusts its conformeric structure to accommodate the new conditions. It is this dynamics, the formation of the cation−π bonded structure with the positively charged amine group leaning toward the aromatic ring, which is likely observed as a decaying electron binding energy in the RFS. The reduced number of minimum energy structures in the ion-like Rydberg state causes the decrease in line width of the 3s signal. A quantitative population distribution analysis, such as the ones we performed in dimethylbutanamine[25] and in triethylamine,[33] was not feasible for PENNA because of the overlap of the spectral signatures of the structural distributions. We note, however, that CENNA shows a time-independent 3s binding energy spectrum, indicating a relatively constant conformer distribution before and after excitation to the Rydberg level. Indeed, no cation−π like interaction is expected between the amine group and the saturated hexyl ring (Figure 7), while steric interactions between the hydrogen atoms of the ring and the methyl groups reduce the structural flexibility of the CENNA molecule.

Conclusions

Because of its two separate but coupled functional groups, PENNA has frequently been used as a model for peptide systems. Contrasting PENNA to the monofunctional CENNA system, our study of energy flow and structural dynamics in highly excited Rydberg states provides an in-depth view of the time scales and relevance of competing energy distribution processes.

Upon excitation to 3p, both PENNA and CENNA experience a rapid decay to the lower 3s electronic level, a purely electronic decay that is accompanied by the orthogonal structural planarization of the amine group. Since the structural motions happen with the same rate in the two molecules while the time constants for electronic relaxation differ by a factor of 5, it seems reasonable to conclude that the two processes are largely independent of each other.

Both optical excitation and energy relaxation to lower lying electronic levels in PENNA can deposit large amounts of vibrational energy into the amine group. The ensuing vibrational energy relaxation distributes this energy among all of PENNA's coordinates on a time scale of 4.8 ps. This process competes with the decay of the 3s level through a curve crossing to a C−C bond σ^* level, which rapidly dissociates the molecule's α bond. Once the vibrational energy is equidistributed about all the vibrational coordinates, this decay channel is greatly slowed down. For our experimental conditions, we found that while the energy is concentrated near the α bond a total of 13% of the molecules dissociate along the repulsive σ^* coordinate. This mechanism appears equivalent to the ECD mechanism proposed by McLafferty for fragmentation via a high n-Rydberg state through a curve crossing.[1] The similarity of time constants of the vibrational relaxation (5.6 ps) and the conformeric transformation (4.8 ps) suggests that those two processes are highly coupled: the vibrational relaxation populates those states that are identified with a cation−π bonded structure. This structural transformation appears to effectively quench the curve crossing to the repulsive surface.

Acknowledgment. We thank Prof. P. G. Williard and Gerald Kagan for their assistance in the synthesis of CENNA. This project was supported by the Division of Chemical Sciences, Geosciences, and Biosciences, the Office of Basic Energy Sciences, the U.S. Department of Energy by grant number DE-FG02-03ER15452, the Army Research Office, grant # W911NF-08-C-0100, administered through Ryon Technologies, INC., a GAANN fellowship, grant # P200A060058, and the Rhode Island Space Grant.

References and Notes

(1) Breuker, K.; Oh, H.; Lin, C.; Carpenter, B. K.; McLafferty, F. W. *Proc. Natl. Acad. Sci. U.S.A.* **2004**, *101*, 14011–14016.
(2) Tang, X. J.; Thibault, P.; Boyd, R. K. *Anal. Chem.* **1993**, *65*, 2824–2834.
(3) Little, D. P.; Speir, J. P.; Senko, M. W.; O'Connor, P. B.; McLafferty, F. W. *Anal. Chem.* **1994**, *66*, 2809–2815.
(4) Kruger, N. A.; Zubarev, R. A.; Carpenter, B. K.; Kelleher, N. L.; Horn, D. M.; McLafferty, F. W. *Int. J. Mass Spectrom.* **1999**, *182−183*, 1–5.

(5) Zubarev, R. A.; Kelleher, N. L.; McLafferty, F. W. *J. Am. Chem. Soc.* **1998**, *120*, 3265.
(6) Turecek, F. *J. Am. Chem. Soc.* **2003**, *125*, 5954–5963.
(7) Leymarie, N.; Costello, C. E.; O'Connor, P. B. *J. Am. Chem. Soc.* **2003**, *125*, 8949–8958.
(8) Anusiewicz, I.; Berdys-Kochanska, J.; Simons, J. *J. Phys. Chem. A* **2005**, *109*, 5801–5813.
(9) Sawicka, A.; Berdys-Kochanska, J; Skurski, P.; Simons, J. *Int. J. Quantum Chem.* **2005**, *102*, 838–846.
(10) Sobczyk, M.; Simons, J. *Int. J. Mass Spectrom.* **2006**, *253*, 274–280.
(11) Sobczyk, M.; Simons, J. *J. Phys. Chem. B* **2006**, *110*, 7159–7527.
(12) Kemnitz, C. R.; Loewen, M. J. *J. Am. Chem. Soc.* **2007**, *129*, 2521.
(13) Brundle, C. R.; Turner, D. W.; Robin, M. B.; Basch, H. *Chem. Phys. Lett.* **1969**, *3*, 92.
(14) Cheng, W.; Kuthirummal, N.; Gosselin, J. L.; Sølling, T. I.; Weinkauf, R.; Weber, P. M. *J. Phys. Chem. A* **2005**, *109*, 1920–1925, 9.
(15) Weinkauf, R. L. *Resonance Ionization Spectroscopy*: American Institute of Physics: Maryland, 1998; pp 117−124.
(16) Lehr, L.; Horneff, T.; Weinkauf, R.; Schlag, E. W. *J. Phys. Chem. A* **2005**, *109*, 8074–8080.
(17) Weinkauf, R.; Lehr, L.; Metsala, A. *J. Phys. Chem. A* **2003**, *107* (16), 2787–2799.
(18) Bixon, M.; Jortner, J. *J. Chem. Phys.* **1997**, *107*, 5154–5170.
(19) Lehr, L; Horneff, T.; Weinkauf, R.; Schlag, E. W. *J. Phys. Chem. A* **2005**, *109*, 8074–8080.
(20) Bixon, M.; Giese, B.; Wessely, S.; Langenbacher, T.; Michel-Beyerle, M. E.; Jortner, J. *Proc. Natl. Acad. Sci.* **1999**, *96*, 11713–11716, 21.
(21) Kuthirummal, N.; Weber, P. M. *Chem. Phys. Lett.* **2003**, *378*, 647–653.
(22) Gosselin, J. L.; Weber, P. M. *J. Phys. Chem. A* **2005**, *109*, 4899–4904.
(23) Kuthirummal, N.; Weber, P. M. *J. Mol. Struct.* **2006**, *787*, 163–166.
(24) Minitti, M. P.; Cardoza, J. D.; Weber, P. M. *J. Phys. Chem. A* **2006**, *110*, 10212–10218.
(25) Minitti, M. P.; Weber, P. M. *Phys. Rev. Lett.* **2007**, *98*, 253004/1–4.
(26) Rudakov, F. M.; Weber, P. M. *Chem. Phys. Lett.* **2009**, *470*, 187–190.
(27) Gosselin, J. L.; Minitti, M. P.; Rudakov, F. M.; Sølling, T. I.; Weber, P. M. *J. Phys. Chem. A* **2006**, *110*, 4251–4255.
(28) Kim, B.; Thantu, N.; Weber, P. M. *J. Chem. Phys.* **1992**, *97*, 5384.
(29) Cardoza, J. D.; Weber, P. M. *J. Chem. Phys.* **2007**, *127*, 036101/1.
(30) Devereux, J. M.; Payne, K. R.; Peeling, E. R. A. *J. Chem. Soc.* **1957**, 2845–2851.
(31) Cardoza, J. D.; Rudakov, F. M.; Weber, P. M. *J. Phys. Chem. A* **2008**, *112* (43), 10736–10743.
(32) Frisch, M. J.; Trucks, G. W.; Schlegel, H. B.; Scuseria, G. E.; Robb, M. A.; Cheeseman, J. R.; Montgomery, J. A., Jr.; Vreven, T.; Kudin, K. N.; Burant, J. C.; Millam, J. M.; Iyengar, S. S.; Tomasi, J.; Barone, V.; Mennucci, B.; Cossi, M.; Scalmani, G.; Rega, N.; Petersson, G. A.; Nakatsuji, H.; Hada, M.; Ehara, M.; Toyota, K.; Fukuda, R.; Hasegawa, J.; Ishida, M.; Nakajima, T.; Honda, Y.; Kitao, O.; Nakai, H.; Klene, M.; Li, X.; Knox, J. E.; Hratchian, H. P.; Cross, J. B.; Bakken, V.; Adamo, C.; Jaramillo, J.; Gomperts, R.; Stratmann, R. E.; Yazyev, O.; Austin, A. J.; Cammi, R.; Pomelli, C.; Ochterski, J. W.; Ayala, P. Y.; Morokuma, K.; Voth, G. A.; Salvador, P.; Dannenberg, J. J.; Zakrzewski, V. G.; Dapprich, S.; Daniels, A. D.; Strain, M. C.; Farkas, O.; Malick, D. K.; Rabuck, A. D.; Raghavachari, K.; Foresman, J. B.; Ortiz, J. V.; Cui, Q.; Baboul, A. G.; Clifford, S.; Cioslowski, J.; Stefanov, B. B.; Liu, G.; Liashenko, A.; Piskorz, P.; Komaromi, I.; Martin, R. L.; Fox, D. J.; Keith, T.; Al-Laham, M. A.; Peng, C. Y.; Nanayakkara, A.; Challacombe, M.; Gill, P. M. W.; Johnson, B.; Chen, W.; Wong, M. W.; Gonzalez, C.; Pople, J. A. *Gaussian 03*, revision C.02; Gaussian, Inc.: Wallingford, CT, 2004.
(33) Deb, S.; Bayes, B.; Minitti, M. P.; Weber, P. M. Structural Dynamics in Floppy Systems: Ultrafast Conformeric Motions in Rydberg-Excited Triethylamine, submitted for publication.

JP101881X